

PHSD - a microscopic transport approach for strongly interacting systems

E.L. Bratkovskaya, W. Cassing, P. Moreau, L. Oliva, O.E. Soloveva, T. Song

Abstract We present the basic ideas of the Parton-Hadron-String Dynamics (PHSD) transport approach which is a microscopic covariant dynamical model for strongly interacting systems formulated on the basis of Kadanoff-Baym equations for Green's functions in phase-space representation (in 1st order gradient expansion beyond the quasi-particle approximation). The approach consistently describes the full evolution of a relativistic heavy-ion collision from the initial hard scatterings and string formation through the dynamical deconfinement phase transition to the strongly-interacting quark-gluon plasma (sQGP) as well as hadronization and the subsequent interactions in the expanding hadronic phase. The PHSD approach has been applied to p+p, p+A and A+A collisions from lower SIS to LHC energies and been successful in describing a large number of experimental data including single-particle spectra, collective flow and electromagnetic probes. Some highlights of recent PHSD results will be presented.

E.L. Bratkovskaya

GSI Helmholtzzentrum für Schwerionenforschung GmbH, Darmstadt, Germany,
Institut für Theoretische Physik, Goethe-Universität Frankfurt am Main, Germany
e-mail: elena.bratkovskaya@th.physik.uni-frankfurt.de

W. Cassing

Institut für Theoretische Physik, Justus-Liebig-Universität Giessen, Germany
e-mail: wolfgang.cassing@theo.physik.uni-giessen.de

P. Moreau, O.E. Soloveva

Institut für Theoretische Physik, Goethe-Universität Frankfurt am Main, Germany

L. Oliva

Institut für Theoretische Physik, Goethe-Universität Frankfurt am Main, Germany
GSI Helmholtzzentrum für Schwerionenforschung GmbH, Darmstadt, Germany

T. Song

GSI Helmholtzzentrum für Schwerionenforschung GmbH, Darmstadt, Germany

1 Introduction

The phase transition from partonic degrees of freedom (quarks and gluons) to interacting hadrons is a central topic of modern high-energy physics. In order to understand the dynamics and relevant scales of this transition laboratory experiments under controlled conditions are performed with relativistic nucleus-nucleus collisions. Hadronic spectra and relative hadron abundances from these experiments reflect important aspects of the dynamics in the hot and dense zone formed in the early phase of the reaction and collective flows provide information on the transport properties of the medium generated on short time scales. Since relativistic heavy-ion collisions start with impinging nuclei in their groundstates a proper non-equilibrium description of the entire dynamics through possibly different phases up to the final asymptotic hadronic states - eventually showing some degree of equilibration - is mandatory.

About 40 years ago cascade calculations have been employed for the description of nucleus-nucleus collisions in the 1-2 AGeV range [1] which provided already some good idea about the reaction dynamics including essentially nucleons, Δ -resonances, pions and kaons. These calculations have been based on the Boltzmann equation which, however, is entirely classical and lacks quantum statistics appropriate for fermions and bosons. In particular the Pauli blocking for nucleons was found to be essential at lower bombarding energies and cascade calculations were extended in line with the Uehling-Uhlenbeck equation for fermions [2] incorporating also some mean-field potential calculated in Hartree approximation with various two-body Skyrme forces. These type of transport models are denoted as Boltzmann-Uehling-Uhlenbeck (BUU) or Vlasov-Uehling-Uhlenbeck (VUU) models [3, 4] and are still in use nowadays by some groups. Independently, Quantum Molecular Dynamical (QMD) models [5] have been proposed in which the testparticles of the BUU/VUU approaches are replaced by Gaussians allowing for the simulation of single events while keeping the fluctuations. Explicit isospin degrees of freedom have been incorporated in IQMD [6], too. Since these type of models are based on a Hamiltonian with fixed two-body forces one could evaluate the nuclear equation of state (EoS) at zero temperature or in thermal equilibrium and one of the primary issues was to extract the nuclear EoS from heavy-ion data by means of BUU/VUU or QMD calculations. Later on higher baryonic resonances as well as mesons like η , K^\pm , K^0 , \bar{K}^0 , ρ , ω , ϕ have been incorporated which led to coupled-channel BUU (CBBU) approaches.

Apart from adding more hadronic degrees of freedom in BUU/VUU fully relativistic formulations have been carried out on the basis of some Lagrangian density including a selected set of hadronic degrees of freedom [7, 8, 9]. All baryons in such relativistic BUU (RBUU) models were propagated with scalar and vector selfenergies that were matched to reproduce collective flow data from heavy-ion collisions as well as particle spectra. This was a necessary step to go ahead in bombarding energy to ultra-relativistic p+A and A+A collisions, which were studied experimentally at the CERN SPS in the nineties. However, when increasing the number of degrees of freedom and adding high-mass short-lived resonances a lot of ambiguities entered

the RBUU models since the couplings between the different hadronic species were unknown experimentally to a large extent. A way out was to incorporate the particle production by string formation and decay in line with the LUND model [10] which included only a formation time of hadrons ($\tau_F \approx 0.8$ fm/c) and a fragmentation function primarily fitted to hadron spectra from e^+e^- annihilation, where only a single string is formed. Familiar versions are the Hadron-String-Dynamics (HSD) [11, 12] or Ultra-relativistic Quantum Molecular Dynamics (UrQMD) [13] approaches that have been applied to p+A and A+A reactions in a wide range of energies up to the top SPS energy of 158 AGeV. In fact, a direct comparison between these two models for p+p and A+A collisions has provided very similar results for hadron spectra and flows up to $\sqrt{s_{NN}} = 17.3$ GeV [14]. Furthermore, a relativistic extension of the QMD model - based on the NJL Lagrangian - has been proposed in Ref. [15] but not followed up further except for a comparative study in Ref. [16].

By Legendre transformations the Hamiltonian density could be easily evaluated in the RBUU models and the nuclear EoS in thermal (or chemical) equilibrium, accordingly. However, it was soon noticed that with increasing temperature T and baryon density ρ_B (or baryon chemical potential μ_B) the energy density was likely to exceed some critical energy density (~ 1 GeV/fm³) as indicated by early lattice QCD (lQCD) calculations which also showed that with increasing T a restoration of chiral symmetry should happen as seen from the temperature dependence of the scalar quark condensate $\langle \bar{q}q \rangle (T)$. Furthermore, the interaction rates of strongly interacting hadrons reached a couple of hundred MeV at high baryon density ρ_B and temperature T such that the on-shell quasi-particle limit - applied in the standard models - became questionable. Furthermore, the spectral evolution especially of vector mesons in a hot and dense environment became of primary interest since the electromagnetic decay of vector mesons into dilepton pairs could be measured experimentally and was considered as a primary probe for the restoration of chiral symmetry in these media. To this end the relativistic transport approach was extended to off-shell dynamics on the basis of the Kadanoff-Baym dynamics in the turn of the Millennium [17, 18, 19] and it became possible to calculate the in-medium spectroscopy of vector mesons in heavy-ion collisions [20]. On the other hand, experimental observations at the Relativistic Heavy Ion Collider (RHIC) indicated that a new medium (Quark-Gluon Plasma (QGP)) was created in ultrarelativistic Au+Au collisions that is interacting more strongly than hadronic matter. Moreover, in line with theoretical studies in Refs. [21, 22, 23] the QCD medium showed phenomena of an almost perfect liquid of partons [24, 25] as extracted from the strong radial expansion and the scaling of elliptic flow $v_2(p_T)$ of mesons and baryons with the number of constituent quarks and antiquarks [24].

The question about the properties of this (nonperturbative) QGP liquid became of primary interest as well as dynamical concepts describing the formation of color neutral hadrons from colored partons (hadronization). A fundamental issue for hadronization is the conservation of 4-momentum as well as the entropy problem because by fusion/coalescence of massless (or low constituent mass) partons to color neutral bound states of low invariant mass (e.g. pions) the number of degrees of freedom and thus the total entropy is reduced in the hadronization process

[26, 27, 28]. This problem - a violation of the second law of thermodynamics as well as the conservation of four-momentum and flavor currents - has been addressed in Ref. [29] on the basis of the Dynamical QuasiParticle Model (DQPM) employing covariant transition rates for the fusion of massive quarks and antiquarks to color neutral hadronic resonances or strings. The DQPM is an effective field-theoretical model based on covariant propagators for quarks/antiquarks and gluons that have a finite width in their spectral functions (imaginary parts of the propagators). The determination/extraction of complex selfenergies for the partonic degrees of freedom has been performed in Refs. [30, 31] by fitting lattice QCD (lQCD) data within the DQPM and thus extracting a temperature-dependent effective coupling (squared) $g^2(T/T_c)$, where T_c denotes the critical temperature for the phase transition from hadrons to partons. This transition at low baryon chemical potential was found to be a crossover and the critical temperature T_c could be extracted from the lQCD data. In fact, the DQPM allows for a simple and transparent interpretation of lattice QCD results for thermodynamic quantities as well as correlators and leads to effective strongly interacting partonic quasiparticles with broad spectral functions. For a review on off-shell transport theory and results from the DQPM in comparison to lQCD we refer the reader to Refs. [32, 33].

Now a consistent dynamical approach - valid also for strongly interacting systems - could be formulated on the basis of Kadanoff-Baym (KB) equations [17] or off-shell transport equations in phase-space representation, respectively [17, 18, 19]. In the KB theory the field quanta are described in terms of dressed propagators with complex selfenergies (as in the DQPM). Whereas the real part of the selfenergies can be related to mean-field potentials (of Lorentz scalar, vector or tensor type), the imaginary parts provide information about the lifetime and/or reaction rates of time-like particles [32]. Once the proper (complex) selfenergies of the degrees of freedom are known the time evolution of the system is fully governed by off-shell transport equations (as described in Refs. [17, 32]).

2 The PHSD approach

The Parton-Hadron-String-Dynamics approach is a microscopic covariant transport model that incorporates effective partonic as well as hadronic degrees of freedom and involves a dynamical description of the hadronization process from partonic to hadronic matter. Whereas the hadronic part is essentially equivalent to the conventional HSD approach [12] the partonic dynamics is based on the Dynamical Quasiparticle Model [30, 31] which describes QCD properties in terms of single-particle Green's functions in the form

$$G^R(\omega, \mathbf{p}) = \left(\omega^2 - \mathbf{p}^2 - M^2 + 2i\gamma\omega \right)^{-1}, \quad (1)$$

where M denotes the (resummed) mass of the parton and γ its width, while (ω, \mathbf{p}) is the parton four-momentum. With the (essentially three) DQPM parameters for

the temperature-dependent effective coupling $g^2(T/T_c)$ fixed by lattice QCD results the approach is fully defined in the partonic phase. We mention in passing that the off-shell transport equations can be solved within an extended testparticle Ansatz [17, 32].

One might ask whether the quasiparticle properties – fixed in thermal equilibrium – should be appropriate also for the nonequilibrium configurations. This question is nontrivial and can only be answered by detailed investigations e.g. on the basis of Kadanoff-Baym equations. We recall that such studies have been summarized in Ref. [32] for strongly interacting scalar fields that initially are far off-equilibrium and simulate momentum distributions of colliding systems at high relative momentum. The results for the effective parameters M and γ , which correspond to the time-dependent pole mass and width of the propagator (1), indicate that the quasiparticle properties - except for the very early off-equilibrium configuration - are close to the equilibrium mass and width even though the phase-space distribution of the particles is far from equilibrium (cf. Figs. 8 to 10 in Ref. [32]). Accordingly, we will adopt the equilibrium quasiparticle properties also for phase-space configurations out of equilibrium as appearing in relativistic heavy-ion collisions. The reader has to keep in mind that this approximation is well motivated, however, not fully equivalent to the exact solution.

On the hadronic side PHSD includes explicitly the baryon and antibaryon octet and decuplet, the 0^- - and 1^- -meson nonets as well as selected higher resonances as in HSD [12]. Hadrons of higher masses (> 1.5 GeV in case of baryons and > 1.3 GeV in case of mesons) are treated as "strings" (color-dipoles) that decay to the known (low-mass) hadrons according to the JETSET algorithm [10]. We discard an explicit recapitulation of the string formation and decay and refer the reader to the original work [10].

2.1 Hadronization

Whereas the dynamics of partonic as well as hadronic systems is fixed by the DQPM or HSD, respectively, the change in the degrees of freedom has to be specified in line with the lattice QCD equation of state. The hadronization, i.e. the transition from partonic to hadronic degrees of freedom, has been introduced in Refs. [29, 34] and is repeated here for completeness. The hadronization is implemented in PHSD by local covariant transition rates e.g. for $q + \bar{q}$ fusion to a mesonic state m of four-momentum $p = (\omega, \mathbf{p})$ at space-time point $x = (t, \mathbf{x})$:

$$\begin{aligned} \frac{dN_m(x, p)}{d^4x d^4p} &= Tr_q Tr_{\bar{q}} \delta^4(p - p_q - p_{\bar{q}}) \delta^4\left(\frac{x_q + x_{\bar{q}}}{2} - x\right) \omega_q \rho_q(p_q) \omega_{\bar{q}} \rho_{\bar{q}}(p_{\bar{q}}) \\ &\times |v_{q\bar{q}}|^2 W_m(x_q - x_{\bar{q}}, (p_q - p_{\bar{q}})/2) N_q(x_q, p_q) N_{\bar{q}}(x_{\bar{q}}, p_{\bar{q}}) \delta(\text{flavor, color}). \end{aligned} \quad (2)$$

In Eq. (2) we have introduced the shorthand notation,

$$Tr_j = \sum_j \int d^4x_j \int \frac{d^4p_j}{(2\pi)^4}, \quad (3)$$

where \sum_j denotes a summation over discrete quantum numbers (spin, flavor, color); $N_j(x, p)$ is the phase-space density of parton j at space-time position x and four-momentum p . In Eq. (2) $\delta(\text{flavor, color})$ stands symbolically for the conservation of flavor quantum numbers as well as color neutrality of the formed hadronic state m which can be viewed as a color-dipole or "pre-hadron". Furthermore, $v_{q\bar{q}}(\rho_p)$ is the effective quark-antiquark interaction from the DQPM (displayed in Fig. 10 of Ref. [31]) as a function of the local parton ($q + \bar{q} + g$) density ρ_p (or energy density). Furthermore, $W_m(x, p)$ is the dimensionless phase-space distribution of the formed "pre-hadron", i.e.

$$W_m(\xi, p_\xi) = \exp\left(\frac{\xi^2}{2b^2}\right) \exp\left(2b^2(p_\xi^2 - (M_q - M_{\bar{q}})^2/4)\right) \quad (4)$$

with $\xi = x_1 - x_2 = x_q - x_{\bar{q}}$ and $p_\xi = (p_1 - p_2)/2 = (p_q - p_{\bar{q}})/2$. The width parameter b is fixed by $\sqrt{\langle r^2 \rangle} = b = 0.66$ fm (in the rest frame) which corresponds to an average rms radius of mesons. We note that the expression (4) corresponds to the limit of independent harmonic oscillator states and that the final hadron-formation rates are approximately independent of the parameter b within reasonable variations. By construction the quantity (4) is Lorentz invariant; in the limit of instantaneous hadron formation, i.e. $\xi^0 = 0$, it provides a Gaussian dropping in the relative distance squared $(\mathbf{r}_1 - \mathbf{r}_2)^2$. The four-momentum dependence reads explicitly (except for a factor $1/2$)

$$(E_1 - E_2)^2 - (\mathbf{p}_1 - \mathbf{p}_2)^2 - (M_1 - M_2)^2 \leq 0 \quad (5)$$

and leads to a negative argument of the second exponential in Eq. (4) favoring the fusion of partons with low relative momenta $p_q - p_{\bar{q}} = p_1 - p_2$.

Some comments on the hadronization scheme are in order: The probability for a quark to hadronize is essentially proportional to the timestep dt in the calculation, the number of possible hadronization partners in the volume $dV \sim 5$ fm³ and the transition matrix element squared (apart from the gaussian overlap function). For temperatures above T_c the probability is rather small ($\ll 1$) but for temperatures close to T_c and below T_c the matrix element becomes very large since it essentially scales with the effective coupling squared $g^2(T/T_c)$ which is strongly enhanced in the infrared. For a finite timestep dt – as used in the calculations – the probability becomes larger than 1 which implies that the quark has to hadronize with some of the potential antiquarks in the actual timestep if the temperature or energy density becomes too low. Furthermore, the gluons practically freeze out close to T_c since the mass difference between quarks and gluons increases drastically with decreasing temperature and the reaction channel $g \leftrightarrow q + \bar{q}$ is close to equilibrium. This implies that all partons hadronize. Due to numerics some leftover partons may occur at the end of the calculations which are forced to hadronize by increasing the volume dV until they have found a suitable partner. In practice the forced hadronization was

only used for LHC energies where the computational time was stopped at ~ 1000 fm/c when partons with rapidities close to projectile or target rapidity did not yet hadronize due to time dilatation ($\gamma_{cm} \approx 1400$).

Related transition rates (2) are defined for the fusion of three off-shell quarks ($q_1 + q_2 + q_3 \leftrightarrow B$) to a color neutral baryonic (B or \bar{B}) resonances of finite width (or strings) fulfilling energy and momentum conservation as well as flavor current conservation (cf. Ref. [34]). In contrast to the familiar coalescence models this hadronization scheme solves the problem of simultaneously fulfilling all conservation laws and the constraint of entropy production. For further details we refer the reader to Refs. [29, 34].

2.2 Initial conditions

The initial conditions for the parton/hadron dynamical system have to be specified additionally. In order to describe relativistic heavy-ion reactions we start with two nuclei in their semi-classical groundstate, boosted towards each other with a velocity β (in z -direction), fixed by the bombarding energy. The initial phase-space distributions of the projectile and target nuclei are determined in the local Thomas-Fermi limit as in the HSD transport approach [12] or the UrQMD model [13]. We recall that at relativistic energies the initial interactions of two nucleons are well described by the excitation of two color-neutral strings which decay in time to the known hadrons (mesons, baryons, antibaryons) [10]. Initial hard processes - i.e. the short-range high-momentum transfer reactions that can be well described by perturbative QCD - are treated in PHSD (as in HSD) via PYTHIA. The novel element in PHSD (relative to HSD) is the string melting concept as also used in the AMPT model [28] in a similar context. However, in PHSD the strings (or possibly formed hadrons) are only allowed to melt if the local energy density $\epsilon(x)$ (in the local rest frame) is above the transition energy density ϵ_c which in the DQPM is $\epsilon_c \approx 0.5 \text{ GeV/fm}^3$. The mesonic strings then decay to quark-antiquark pairs according to an intrinsic quark momentum distribution,

$$F(\mathbf{q}) \sim \exp(-2b^2\mathbf{q}^2), \quad (6)$$

in the meson rest-frame (cf. Eq. (2) for the inverse process). The parton final four-momenta are selected randomly according to the momentum distribution (6) (with $b=0.66 \text{ fm}$), and the parton-energy distribution is fixed by the DQPM at given energy density $\epsilon(\rho_s)$ in the local cell with scalar parton density ρ_s . The flavor content of the $q\bar{q}$ pair is fully determined by the flavor content of the initial string. By construction the "string melting" to massive partons conserves energy and momentum as well as the flavor content. In contrast to Ref. [28] the partons are of finite mass – in line with their local spectral function – and obtain a random color $c = (1, 2, 3)$ or (r, b, g) in addition. Of course, the color appointment is color neutral, i.e. when selecting a color c for the quark randomly the color for the antiquark is fixed by $-c$. The baryonic strings melt analogously into a quark and a diquark while the diquark, furthermore, decays to two quarks. Dressed gluons are generated by the fusion of

nearest neighbor $q + \bar{q}$ pairs ($q + \bar{q} \rightarrow g$) that are flavor neutral until the ratio of gluons to quarks reaches the value $N_g/(N_q + N_{\bar{q}})$ given by the DQPM for the energy density of the local cell. This recombination is performed for all cells in space during the passage time of the target and projectile (before the calculation continues with the next timestep) and conserves the four-momentum as well as the flavor currents. We note, however, that the initial phase in PHSD is dominated by quark and antiquark degrees of freedom[35].

Apart from proton-proton, proton-nucleus or nucleus-nucleus collisions the PHSD approach can also be employed to study the properties of the interacting hadron/parton system in a finite box with periodic boundary conditions [39]. To this aim the system is initialized by a homogeneous distribution of test-particles in a finite box with a momentum distribution close to a thermal one. Note that in PHSD the system cannot directly be initialized by a temperature and chemical potential since these Lagrange parameters can only be determined when the system has reached a thermal and chemical equilibrium, i.e. when all forward and backward reaction rates have become equal; this is easy to check in the transport simulations.

2.3 Partonic cross sections

On the partonic side the following elastic and inelastic interactions are included in PHSD $qq \leftrightarrow qq$, $\bar{q}\bar{q} \leftrightarrow \bar{q}\bar{q}$, $gg \leftrightarrow gg$, $gg \leftrightarrow g$, $q\bar{q} \leftrightarrow g$, $qg \leftrightarrow qg$, $g\bar{q} \leftrightarrow g\bar{q}$ exploiting detailed-balance with cross sections calculated from the leading Feynman diagrams employing the effective propagators and couplings $g^2(T/T_c)$ from the DQPM [37]. As an example we show in Fig. 1 the leading order Feynman diagrams for the $qq' \rightarrow qq'$ and $q\bar{q} \rightarrow q'\bar{q}'$ processes.

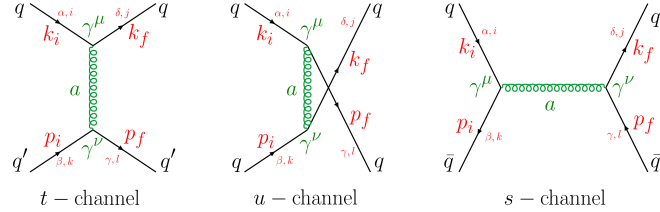


Fig. 1 Leading order Feynman diagrams for the $qq' \rightarrow qq'$ and $q\bar{q} \rightarrow q'\bar{q}'$ processes. The initial and final 4-momenta are k_i and p_i , and k_f and p_f , respectively. The indices $i, j, k, l = 1 - 3$ denote the quark colors, $a = 1 - 8$ the gluon colors while the quark flavor is indicated by the indices $\alpha, \beta, \delta, \gamma = u, d, s, \dots$

Partonic reactions such as $g + q \leftrightarrow q$ or $g + g \leftrightarrow q + \bar{q}$ have been discarded in the present calculations due to their low rates since the large mass of the gluon leads to a strong mismatch in the energy thresholds between the initial and final channels. In this case q stands for the 4 lightest quarks (u, d, s, c). Furthermore, the evaluation of photon and dilepton production is calculated perturbatively and

channels like $g + q \rightarrow q + \gamma$ are included. In this case the probability for photon (dilepton) production from each channel is added up and integrated over space and time [33] without introducing any new parameter in the PHSD approach since the electromagnetic coupling is well known.

Numerical tests of the parton dynamics with respect to conservation laws, interaction rates in and out-of equilibrium in a finite box with periodic boundary conditions have been presented in Ref. [39]. In fact, in Ref. [39] it was shown that the PHSD calculations in the box give practically the same results in equilibrium as the DQPM. We note in passing that the total energy is conserved in the box calculations up to about 3 digits while in the heavy-ion collisions addressed here in the following the violation of energy conservation is typically less than 1 % [34].

3 Transport properties of the partonic system

The starting point to evaluate viscosity coefficients of partonic matter is the Kubo formalism [38] which was also used to calculate the viscosities within the PHSD in a box with periodic boundary conditions (cf. Ref. [36]). We focus here on the calculation of the shear viscosity based on Ref. [40] which reads:

$$\begin{aligned} \eta^{\text{Kubo}}(T, \mu_q) &= - \int \frac{d^4 p}{(2\pi)^4} p_x^2 p_y^2 \sum_{i=q,\bar{q},g} d_i \frac{\partial f_i(\omega)}{\partial \omega} \rho_i(\omega, \mathbf{p})^2 \\ &= \frac{1}{15T} \int \frac{d^4 p}{(2\pi)^4} \mathbf{p}^4 \sum_{i=q,\bar{q},g} d_i ((1 \pm f_i(\omega)) f_i(\omega)) \rho_i(\omega, \mathbf{p})^2, \end{aligned} \quad (7)$$

where the notation $f_i(\omega) = f_i(\omega, T, \mu_q)$ is used for the distribution functions, and ρ_i denotes the spectral function of the partons, while d_i stand for the degeneracy factors. We note that the derivative of the distribution function accounts for the Pauli-blocking (-) and Bose-enhancement (+) factors. Following Ref. [41], we can evaluate the integral over $\omega = p_0$ in Eq. (7) by using the residue theorem. When keeping only the leading order contribution in the width $\gamma(T, \mu_B)$ from the residue - evaluated at the poles of the spectral function $\omega_i = \pm \tilde{E}(\mathbf{p}) \pm i\gamma$ - we finally obtain:

$$\eta^{\text{RTA}}(T, \mu_q) = \frac{1}{15T} \int \frac{d^3 p}{(2\pi)^3} \sum_{i=q,\bar{q},g} \frac{\mathbf{p}^4}{E_i^2 \Gamma_i(\mathbf{p}, T, \mu_q)} d_i ((1 \pm f_i(E_i)) f_i(E_i)), \quad (8)$$

which corresponds to the expression derived in the relaxation-time approximation (RTA) [42] by identifying the interaction rate Γ with 2γ as expected from transport theory in the quasiparticle limit [43]. We recall that γ is the width parameter in the parton propagator (1). The interaction rate $\Gamma_i(\mathbf{p}, T, \mu_q)$ (inverse relaxation time) is calculated microscopically from the collision integral using the differential cross sections for parton scattering as described in Section 2.3. We, furthermore, recall that the pole energy is $E_i^2 = p^2 + M_i^2$ where M_i is the pole mass given in the DQPM.

We use here the notation $\sum_{j=q,\bar{q},g}$ which includes the contribution from all possible partons which in our case are the gluons and the (anti-)quarks of three different flavors (u, d, s).

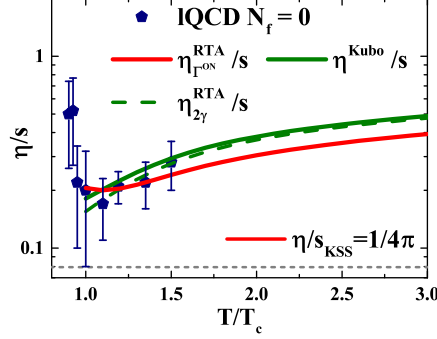


Fig. 2 The ratio of shear viscosity to entropy density as a function of the scaled temperature T/T_c for $\mu_B = 0$ from Eq. (7-8). The solid green line (η^{Kubo}/s) shows the results from the original DQPM in the Kubo formalism while the dashed green line ($\eta_{2\gamma}^{\text{RTA}}/s$) shows the same result in the quasiparticle approximation (8). The solid red line ($\eta_{\Gamma^{\text{on}}}^{\text{RTA}}/s$) results from Eq. (8) using the interaction rate Γ^{on} calculated by the microscopic differential cross sections in the on-shell limit. The dashed gray line demonstrates the Kovtun-Son-Starinets bound [44] $(\eta/s)_{\text{KSS}} = 1/(4\pi)$, and the symbols show IQCD data for pure SU(3) gauge theory obtained within the Backus-Gilbert method taken from Ref. [45] (pentagons).

The actual results are displayed in Fig. 2 for the ratio of shear viscosity to entropy density η/s as a function of the scaled temperature T/T_c for $\mu_B = 0$ in comparison to those from lattice QCD [45]. The solid green line (η^{Kubo}/s) shows the result from the original DQPM in the Kubo formalism while the dashed green line ($\eta_{2\gamma}^{\text{RTA}}/s$) shows the same result in the relaxation-time approximation (8) by replacing Γ_i by $2\gamma_i$. The solid red line ($\eta_{\Gamma^{\text{on}}}^{\text{RTA}}/s$) results from Eq. (8) using the interaction rate Γ^{on} calculated by the microscopic differential cross sections in the on-shell limit. We find that - apart from temperatures close to T_c - the ratios η/s do not differ very much and have a similar behavior as a function of temperature. The approximation (8) of the shear viscosity is found to be very close to the one from the Kubo formalism (7) indicating that the quasiparticle limit ($\gamma \ll M$) holds in the DQPM.

An overview for the ratio of shear viscosity to entropy density η/s as a function of the scaled temperature $T/T_c(\mu_B)$ and μ_B is given Fig. 3 in case of the Kubo formalism (a) (7) and the relaxation-time approximation (8) (b). There is no strong variation with μ_B for fixed $T/T_c(\mu_B)$, however, the ratio increases slightly with μ_B in the on-shell limit while it slightly drops with μ_B in the Kubo formalism for the DQPM. Accordingly, there is some model uncertainty when extracting the shear viscosity in the different approximations.

In summarizing this section we find that the results for the ratio of shear viscosity over entropy density from the original DQPM and those from the microscopic calculations are similar and within error bars compatible with present results from

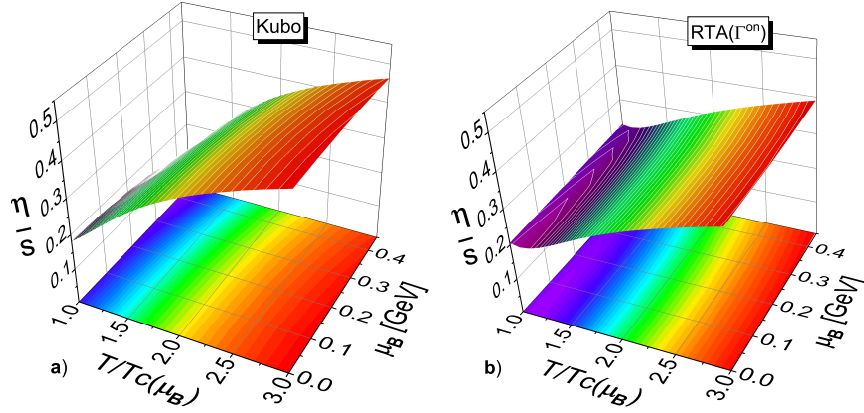


Fig. 3 The ratio of shear viscosity to entropy density η/s as a function of the scaled temperature $T/T_c(\mu_B)$ and baryon chemical potential μ_B calculated within the Kubo formalism (a) from Eq. (7) and in the Relaxation Time Approximation (RTA) (b) from Eq. (8) using the on-shell interaction rate Γ^{on} .

lattice QCD. However, having the differential cross sections for each partonic channel at hand one might find substantial differences for non-equilibrium configurations as encountered in relativistic heavy-ion collisions where a QGP is formed initially out-of-equilibrium.

4 Observables from relativistic nucleus-nucleus collisions

We briefly report on results from PHSD calculations at lower and intermediated energies covered experimentally by the AGS (BNL) and SPS (CERN) with a focus on central Au+Au or Pb+Pb collisions. In this energy range the average baryon chemical potential μ_B is essentially finite - contrary to RHIC and LHC energies - and one might find some traces of the explicit μ_B dependence of the partonic cross sections in observables. To this end we compare results for the rapidity distributions from the PHSD calculations based on the default DQPM parameters (PHSD4.0) [46] with the new PHSD5.0 including the differential partonic cross sections for the individual partonic channels at finite T and μ_B (cf. Ref. [37]). A comparison to the available experimental data is included (for orientation) but not discussed explicitly since this has been done in more detail in Ref. [46]. When implementing the differential cross sections and parton masses into the PHSD5.0 approach one has to specify the Lagrange parameters T and μ_B in each computational cell in space-time. This has been done by employing the DQPM equation of state, which is practically identical to the lattice QCD equation of state, and a diagonalization of the energy-momentum tensor from PHSD as described in Ref. [37].

Fig. 4 displays the actual results for hadronic rapidity distributions in case of 5% central Au+Au collisions at 10.7 AGeV for PHSD4.0 (green dot-dashed lines),

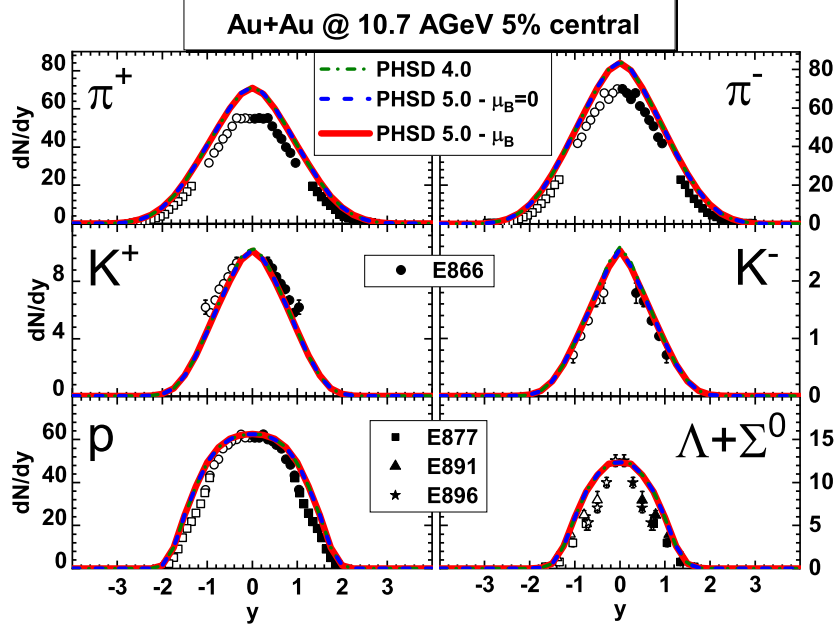


Fig. 4 The rapidity distributions for 5% central Au+Au collisions at 10.7 AGeV for PHSD4.0 (green dot-dashed lines), PHSD5.0 with partonic cross sections and parton masses calculated for $\mu_B = 0$ (blue dashed lines) and with cross sections and parton masses evaluated at the actual chemical potential μ_B in each individual space-time cell (red lines) in comparison to the experimental data from the E866 [47], E877 [48], E891 [49], E877 [50] and E896 [51] collaborations. All PHSD results are the same within the linewidth.

PHSD5.0 with partonic cross sections and parton masses calculated for $\mu_B = 0$ (blue dashed lines), and with cross sections and parton masses evaluated at the actual chemical potential μ_B in each individual space-time cell (red lines) in comparison to the experimental data from the E866 [47], E877 [48], E891 [49], E877 [50] and E896 [51] collaborations. Here we focus on the most abundant hadrons, i.e. pions, kaons, protons and neutral hyperons. We note in passing that the effects of chiral symmetry restoration are incorporated as in Ref. [46] since this was found to be mandatory to achieve a reasonable description of the strangeness degrees of freedom reflected in the kaon and neutral hyperon dynamics. As seen from Fig. 4 there is no difference in rapidity distributions for all the hadron species from the different versions of PHSD within linewidth which implies that there is no sensitivity to the new partonic differential cross sections and parton masses employed. One could argue that this result might be due to the low amount of QGP produced at this energy but the different PHSD calculations for 5% central Pb+Pb collisions at 30 AGeV in Fig. 5 for the hadronic rapidity distributions do not provide a different picture, too. Only when stepping up to the top SPS energy of 158 AGeV one can identify a small difference in the antibaryon sector (\bar{p} , $\bar{\Lambda} + \bar{\Sigma}^0$) in case of 5% central Pb+Pb collisions (cf. Fig. 6).

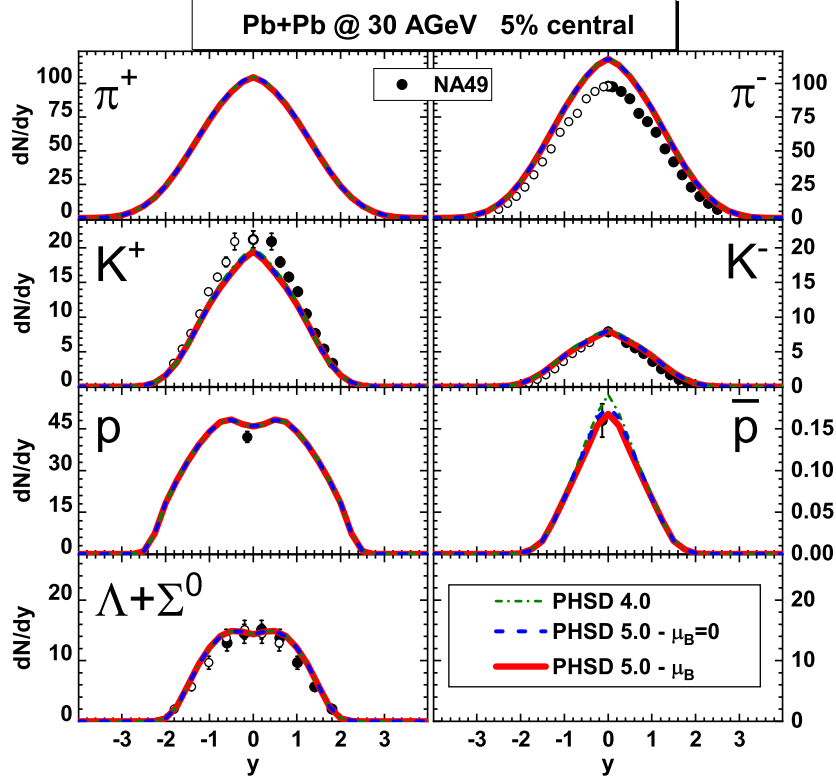


Fig. 5 The rapidity distributions for 5% central Pb+Pb collisions at 30 AGeV for PHSD4.0 (green dot-dashed lines), PHSD5.0 with partonic cross sections and parton masses calculated for $\mu_B = 0$ (blue dashed lines) and with cross sections and parton masses evaluated at the actual chemical potential μ_B in each individual space-time cell (red lines) in comparison to the experimental data from the NA49 Collaboration [52, 53, 54]. All PHSD results are practically the same within the linewidth.

5 Summary

In this contribution we have described the PHSD transport approach [33] and its recent extension to PHSD5.0 [37] to incorporate differential "off-shell" cross sections for all binary partonic channels that are based on the same effective propagators and couplings as employed in the QGP equation of state and the parton propagation. To this end we have recalled the extraction of the partonic masses and the coupling g^2 from lattice QCD data (within the DQPM) and calculated the partonic differential cross sections as a function of T and μ_B for the leading tree-level diagrams (cf. Appendices of Ref. [37]). Furthermore, we have used these differential cross sections to evaluate partonic scattering rates $\Gamma_i(T, \mu_B)$ for fixed T and μ_B as well as to compute the ratio of the shear viscosity η to entropy density s within the Kubo formalism in comparison to calculations from lQCD. It turns out that the ratio η/s calculated with

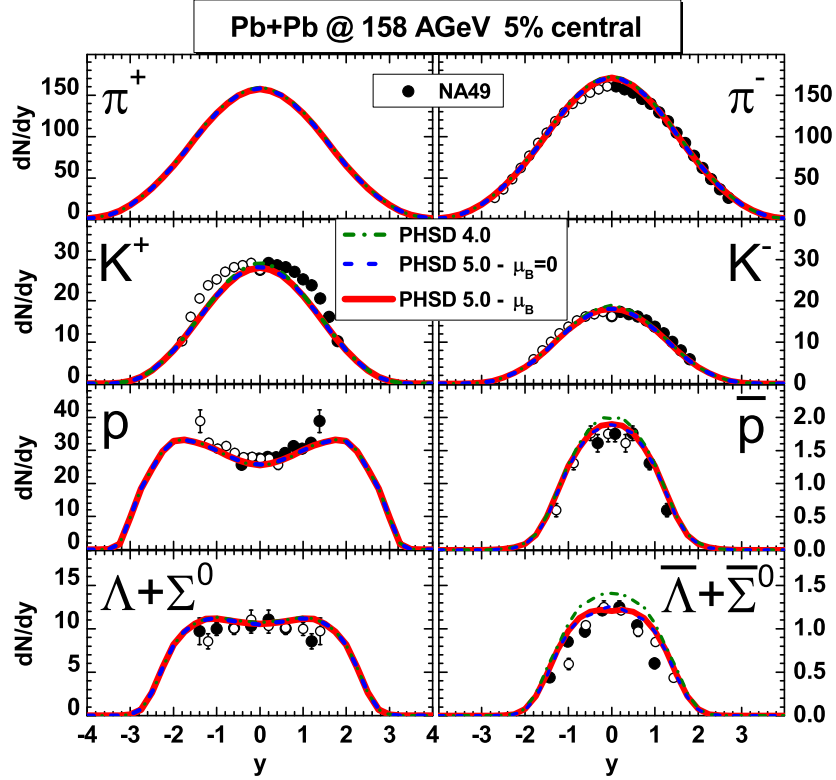


Fig. 6 The rapidity distributions for 5% central Pb+Pb collisions at 158 AGeV for PHSD4.0 (green dot-dashed lines), PHSD5.0 with partonic cross sections and parton masses calculated for $\mu_B = 0$ (blue dashed lines) and with cross sections and parton masses evaluated at the actual chemical potential μ_B in each individual space-time cell (red lines) in comparison to the experimental data from the NA49 Collaboration [55, 56, 57, 58]. All PHSD results are the same within the linewidth except for the antibaryons.

the partonic scattering rates in the relaxation-time approximation is very similar to the original result from the DQPM and to IQCD results such that the present extension of the PHSD approach does not lead to different partonic transport properties. We recall that the novel PHSD version (PHSD5.0) is practically parameter free in the partonic sector since the effective coupling (squared) is determined by a fit to the scaled entropy density from IQCD. The dynamical masses for quarks and gluons then are fixed by the HTL expressions. The interaction rate in the time-like sector is, furthermore, calculated in leading order employing the DQPM propagators and coupling.

When implementing the differential cross sections and parton masses into the PHSD5.0 approach one has to specify the Lagrange parameters T and μ_B in each computational cell in space-time. This has been done by employing the DQPM equation of state, which is practically identical to the lattice QCD equation of state,

and a diagonalization of the energy-momentum tensor from PHSD as described in Ref. [37].

In Section 4 we then have calculated 5% central Au+Au (or Pb+Pb) collisions and compared the results for hadronic rapidity distributions from the previous PHSD4.0 with the novel version PHSD5.0 (with and without the explicit dependence of the partonic differential cross sections and parton masses on μ_B). No differences for all the hadron bulk observables from the various PHSD versions have been found at AGS and FAIR/NICA energies within linewidth which implies that there is no sensitivity to the new partonic differential cross sections employed. Only in case of the kaons and the antibaryons \bar{p} and $\bar{\Lambda} + \bar{\Sigma}^0$, a small difference between PHSD4.0 and PHSD5.0 could be seen at top SPS energy, however, no clear difference between the PHSD5.0 calculations with partonic cross sections for $\mu_B = 0$ and actual μ_B in the local cells.

Our findings can be understood as follows: The fact that we find only small traces of the μ_B -dependence of partonic scattering dynamics in heavy-ion bulk observables - although the differential cross sections and parton masses clearly depend on μ_B - means that one needs a sizable partonic density and large space-time QGP volume to explore the dynamics in the QGP phase. These conditions are only fulfilled at high bombarding energies (top SPS, RHIC energies) where, however, μ_B is rather low. On the other hand, decreasing the bombarding energy to FAIR/NICA energies and, thus, increasing μ_B , leads to collisions that are dominated by the hadronic phase where the extraction of information about the parton dynamics will be rather complicated based on bulk observables. Further investigations of other observables (such as flow coefficients v_n of particles and antiparticles, fluctuations and correlations) might contain more visible μ_B -traces from the QGP phase.

Acknowledgements The authors acknowledge inspiring discussions with J. Aichelin, H. Berrehrah, C. Ratti, E. Seifert, A. Palmese and T. Steinert. This work was supported by the LOEWE center "HIC for FAIR". Furthermore, P.M., L.O. and E.B. acknowledge support by the Deutsche Forschungsgemeinschaft (DFG, German Research Foundation) through the grant CRC-TR 211 'Strong-interaction matter under extreme conditions' - Project number 315477589 - TRR 211. O.S. acknowledges support from HGS-HIRe for FAIR; L.O. and E.B. thank the COST Action THOR, CA15213. The computational resources have been provided by the LOEWE-Center for Scientific Computing.

References

1. J. Cugnon, Phys. Rev. C22, 1885 (1980).
2. E. A. Uehling and G. E. Uhlenbeck, Phys. Rev. 43, 552 (1932).
3. G. F. Bertsch and S. Das Gupta, Phys. Rept. 160, 189 (1988).
4. W. Cassing, V. Metag, U. Mosel, and K. Niita, Phys. Rept. 188, 363 (1990).
5. J. Aichelin and H. Stöcker, Phys. Lett. B176, 14 (1986).
6. C. Hartnack, K. Puri Rajeev, J. Aichelin, Konopka J., S.A. Bass, Horst Stöcker, and W. Greiner, Eur. Phys. J. A1, 151-169 (1998).
7. C.M. Ko, Q. Li, and Ren-Chuan Wang, Phys. Rev. Lett. 59, 1084 (1987).
8. B. Blaettel, V. Koch, W. Cassing, and U. Mosel, Phys. Rev. C38, 1767 (1988).

9. Tomoyuki Maruyama, Wolfgang Cassing, Ulrich Mosel, Stefan Teis, Klaus Weber, Nucl.Phys. A573, 653-675 (1994).
10. H.-U. Bengtsson and T. Sjöstrand, Comp. Phys. Commun. 46, 43 (1987).
11. W. Ehehalt and W. Cassing, Nucl. Phys. A602, 449 (1996).
12. W. Cassing and E. L. Bratkovskaya, Phys. Rep. 308, 65 (1999).
13. S. A. Bass et al., Prog. Part. Nucl. Phys. 41, 255-369 (1998).
14. E.L. Bratkovskaya, M. Bleicher, M. Reiter, S. Soff, H. Stöcker, M. van Leeuwen, S.A. Bass, W. Cassing, Phys. Rev. C69, 054907 (2004).
15. R. Marty and J. Aichelin, Phys. Rev. C87, 034912 (2013).
16. R. Marty, E. Bratkovskaya, W. Cassing, and J. Aichelin, Phys. Rev. C92, 015201 (2015).
17. S. Juchem, W. Cassing and C. Greiner, Phys. Rev. D 69, 025006 (2004); Nucl. Phys. A 743, 92 (2004).
18. W. Cassing and S. Juchem, Nucl. Phys. A 665 (2000) 377; *ibid* A 672, 417 (2000).
19. Y. B. Ivanov, J. Knoll and D. N. Voskresensky, Nucl. Phys. A 672, 313 (2000).
20. E.L. Bratkovskaya and W. Cassing, Nucl. Phys. A807, 214 (2008).
21. E. Shuryak, Prog. Part. Nucl. Phys. 53, 273 (2004).
22. M. H. Thoma, J. Phys. G 31, L7 (2005); Nucl. Phys. A 774, 307 (2006).
23. A. Peshier and W. Cassing, Phys. Rev. Lett. 94, 172301 (2005).
24. I. Arsene *et al.*, Nucl. Phys. A 757, 1 (2005); B. B. Back *et al.*, Nucl. Phys. A 757, 28 (2005); J. Adams *et al.*, Nucl. Phys. A 757, 102 (2005); K. Adcox *et al.*, Nucl. Phys. A 757 184, (2005).
25. T. Hirano and M. Gyulassy, Nucl. Phys. A 769, 71 (2006).
26. R. C. Hwa and C. B. Yang, Phys. Rev. C 67, 034902 (2003); V. Greco, C. M. Ko and P. Levai, Phys. Rev. Lett. 90, 202302 (2003).
27. R. J. Fries, B. Müller, C. Nonaka and S. A. Bass, Phys. Rev. Lett. 90, 202303 (2003).
28. Z.-W. Lin *et al.*, Phys. Rev. C 72, 064901 (2005).
29. W. Cassing and E. L. Bratkovskaya, Phys. Rev. C 78, 034919 (2008).
30. W. Cassing, Nucl. Phys. A 791, 365 (2007).
31. W. Cassing, Nucl. Phys. A 795, 70 (2007).
32. W. Cassing, E. Phys. J. ST 168, 3 (2009).
33. O. Linnyk, E.L. Bratkovskaya, and W. Cassing, Prog. Part. Nucl. Phys. 87, 50 (2016).
34. W. Cassing and E. L. Bratkovskaya, Nucl. Phys. A 831, 215 (2009).
35. P. Moreau, O. Linnyk, W. Cassing, and E. Bratkovskaya, Phys. Rev. C93, 044916 (2016).
36. V. Ozvenchuk, O. Linnyk, M. I. Gorenstein, E. L. Bratkovskaya, and W. Cassing, Phys. Rev. C 87, 024901 (2013).
37. P. Moreau, O. Soloveva, L. Oliva, T. Song, W. Cassing, and E. Bratkovskaya, Phys. Rev. C 100, 014911 (2019).
38. R. Kubo, J. Phys. Soc. Jpn. 12, 570 (1957).
39. V. Ozvenchuk, O. Linnyk, M. I. Gorenstein, E. L. Bratkovskaya, and W. Cassing, Phys. Rev. C 87, 064903 (2013).
40. G. Aarts and J. M. Martinez Resco, J. High Energy Phys. 04, 053 (2002).
41. R. Lang, N. Kaiser, and W. Weise, Eur. Phys. J. A 48, 109 (2012).
42. C. Sasaki and K. Redlich, Phys. Rev. C 79, 055207 (2009).
43. J.-P. Blaizot and E. Iancu, Nucl. Phys. B 557, 183 (1999).
44. P. K. Kovtun, D. T. Son, and A. O. Starinets, Phys. Rev. Lett. 94, 111601 (2005).
45. N. Astrakhantsev, V. Braguta, and A. Kotov, J. High Energy Phys. 04, 101 (2017).
46. A. Palmese, W. Cassing, E. Seifert, T. Steinert, P. Moreau, and E. L. Bratkovskaya, Phys. Rev. C 94, 044912 (2016).
47. Y. Akiba et al. (E802 Collaboration), Nucl. Phys. A 610, 139 (1996).
48. R. Lacasse et al. (E877 Collaboration), Nucl. Phys. A 610, 153 (1996).
49. S. Ahmad et al., Phys. Lett. B 382, 35 (1996); 386, 496(E) (1996).
50. J. Barrette et al. (E877 Collaboration), Phys. Rev. C 63, 014902 (2001).
51. S. Albergo et al., Phys. Rev. Lett. 88, 062301 (2002).
52. C. Alt et al. (NA49 Collaboraion), Phys. Rev. C 73, 044910 (2006).
53. C. Alt et al. (NA49 Collaboration), Phys. Rev. C 77, 024903 (2008).
54. C. Alt et al. (NA49 Collaboration), Phys. Rev. C 78, 034918 (2008).

55. S. V. Afanasiev et al. (NA49 Collaboration), Phys. Rev. C 66, 054902 (2002).
56. T. Anticic et al. (NA49 Collaboration), Phys. Rev. Lett. 93, 022302 (2004).
57. T. Anticic et al. (NA49 Collaboration), Phys. Rev. C 83, 014901 (2011).
58. T. Anticic et al. (NA49 Collaboration), Phys. Rev. C 86, 054903 (2012).